



ELSEVIER

Contents lists available at ScienceDirect

Atmospheric Research

journal homepage: www.elsevier.com/locate/atmosres

Characterization of particle size distributions during winter haze episodes in urban air



Yan Cheng^{a,b,*}, Lu Yan^a, Yu Huang^{b,c}, Qiyuan Wang^{b,c}, Lidia Morawska^{d,**}, Zhaolin Gu^a, Junji Cao^{b,c}, Liyuan Zhang^e, Bowei Li^a, Yelin Wang^a

^a School of Human Settlements and Civil Engineering, Xi'an Jiaotong University, Xi'an, Shaanxi, China

^b State Key Laboratory of Loess and Quaternary Geology, Institute of Earth Environment, Chinese Academy of Sciences, Xi'an 710061, China

^c Key Laboratory of Aerosol Chemistry and Physics, Institute of Earth Environment, Chinese Academy of Sciences, Xi'an 710061, China

^d International Laboratory for Air Quality and Health, Queensland University of Technology, Brisbane, QLD 4001, Australia

^e School of Environmental Science and Engineering, Chang'an University, Xi'an, China

ARTICLE INFO

Keywords:

Particle number concentration (PNC)
Particle number size distribution (PNSD)
New particle formation (NPF)
Haze

ABSTRACT

Detail characterization of particle size distribution and its temporal evolution is one of the critical elements towards uncovering mechanisms behind haze formation, yet rarely conducted. To address this deficiency, we conducted comprehensive characterization of particle size distribution during winter in Xi'an, China. Real-time measurements were conducted using a TSI Fast Mobility Particle Sizer Model 3091 (FMPS, from 5.6 to 523 nm) in the Qujiang campus of Xi'an Jiaotong University in the period from December 4th, 2015 to January 8th, 2016. The FMPS readings were adjusted by factors derived from an intercomparison with a TSI Scanning Mobility Particle Sizer (consisting of a TSI DMA 3081 and a CPC 3772, from 15.1 to 850.8 nm). Seven haze episodes and two new particle formation episodes were recorded during the sampling campaign. Two (E1 and E6) of the seven haze episodes are investigated in this study. E1 was an prolonged episode starting from a new particle formation (NPF) episode, followed by low, sustained PM_{2.5} increase at an average growth rate of 2 μg m⁻³ per hour (from 37 μg m⁻³ to 262 μg m⁻³ within 155 h), while E6 was a short-term haze episode starting from a rapid increase in PM_{2.5} at an rapid growth rate of 27 μg m⁻³ (from 79 μg m⁻³ to 213 μg m⁻³ within only 5 h). The average total particle number concentrations (PNC) were 3.35 × 10⁴ cm⁻³, 4.14 × 10⁴ cm⁻³ and 3.99 × 10⁴ cm⁻³ during normal days, E1, and E6, respectively, showing an increase in particle number concentration from normal days to haze days (*p* < .000 for E1 and *p* < .002 for E6, two-tailed *t*-test). While statically significant, the magnitude of the increase was not as large as of the increase in PM_{2.5} concentration. On normal days, the peak in particle number size distribution (PNSD) was centered at smaller particle sizes (around 60–70 nm, computed based on a normal distribution) and shifted towards larger sizes during the night (139 nm at 0:00 and 168 nm at 4:00 am). The diurnal variations of PNSD during E1 and E6 episodes were not as evident as the variations on normal days, with the centers of the major peaks at 179 nm for E1 and 137 nm for E6. It was found that significant changes in PNC and PNSD occurred during the PM_{2.5} increase phase of severe haze episodes, but not during the high concentration phase. Since the growth rates of PM_{2.5} varied during increase phase between E1 and E6, PM_{2.5} pollution formation mechanisms were different throughout evaluating growth rates as it relates to PM_{2.5}, gaseous pollutants, PNC, PNSD, and meteorological variables in these processes.

1. Introduction

In recent years, China's ever-increasing air pollution problem has attracted worldwide attention. Most large cities in China, including Beijing, Shanghai and, Guangzhou have experienced in the past decades an increasing occurrence of haze episodes (Ding and Liu, 2014; Zhang

et al., 2012), characterized by rapidly increasing PM_{2.5} (mass concentration of particulate matter with aerodynamic diameters < 2.5 μm) and low visibility (Huang et al., 2014; Zhang et al., 2015a; Zhao et al., 2013). Severe haze episodes, especially persistent haze, have put human health at great risk (Lu et al., 2015), and this motivated global interest in investigating such episodes and their drivers. Chemical

* Corresponding author at: School of Human Settlements and Civil Engineering, Xi'an Jiaotong University, Xi'an, Shaanxi, China.

** Corresponding author.

E-mail address: chengyan@mail.xjtu.edu.cn (Y. Cheng).

<https://doi.org/10.1016/j.atmosres.2019.04.033>

Received 14 September 2018; Received in revised form 12 April 2019; Accepted 29 April 2019

Available online 10 May 2019

0169-8095/ © 2019 Elsevier B.V. All rights reserved.

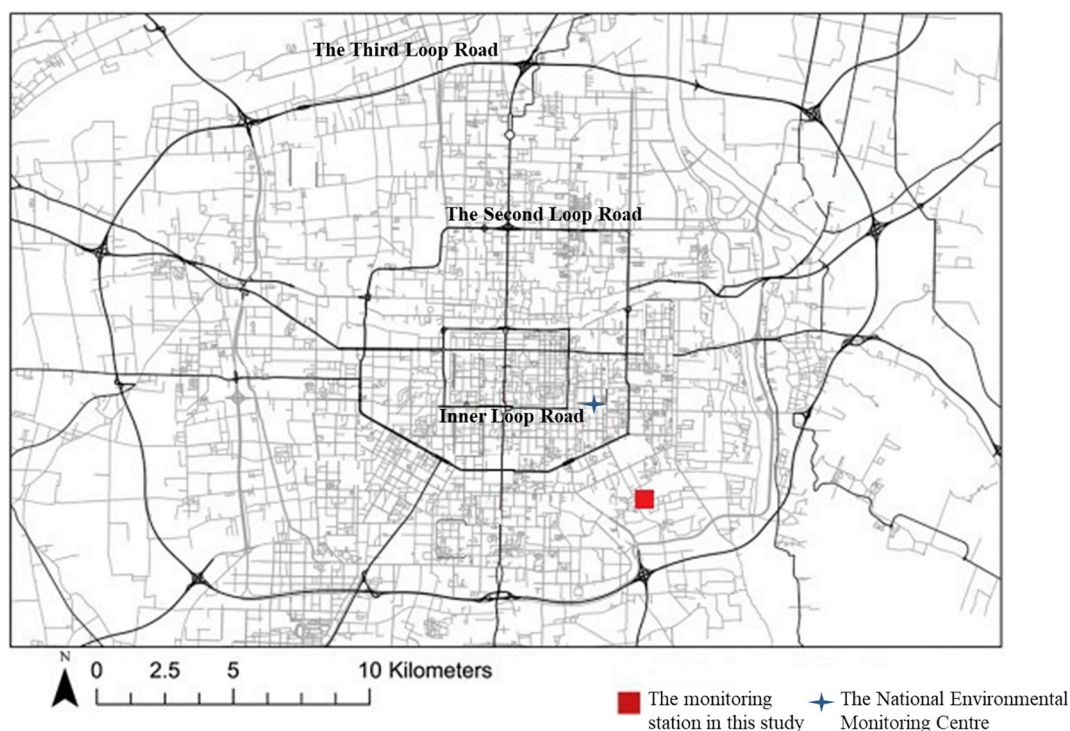


Fig. 1. Location of the monitoring station in Xi'an city.

composition of haze aerosols has been extensively studied and it was demonstrated that it significantly and quickly changes, with the increase in secondary sulfate and nitrate aerosols (Huang et al., 2014; Shang et al., 2018; Tan et al., 2016; Wang et al., 2017a; Wang et al., 2018; Zhang et al., 2015b; Zhang et al., 2016; Zhao et al., 2013; Yang et al., 2013) or organic aerosols (Li et al., 2017).

Only a few studies investigated the number concentrations of haze aerosols. Wang et al. (2014a) reported that particle number size distributions (PNSD) during light and moderate haze episodes were very similar, while the peak during severe haze shifted to larger sizes. During severe haze episodes, the number concentration of particles smaller than 50 nm decreased, while the concentrations of particles in the size ranges of 50–100 nm, 100–200 nm and 0.5–1 μm increased (Guo et al., 2014; Wang et al., 2014a, 2014b; Zhang et al., 2011). In Shanghai, Aitken mode was dominant in PNSD under relatively low pollution conditions, but accumulation mode dominated under prolonged haze and fog days, with a larger peak diameter and higher particle number concentration (PNC) than on relatively low pollution days (Shen et al., 2015; Wang et al., 2014c). New particle formation (NPF) episodes have been frequently observed in many urban areas of China (Peng et al., 2014) and consistently occur prior to polluted periods with a periodic cycle of 4–7 days in Beijing (Guo et al., 2014; Zhang et al., 2015b). The efficient aerosol nucleation and growth in Beijing are attributable to highly elevated concentrations of gaseous aerosol precursors, in particular anthropogenic volatile organic compounds (VOCs), NO_x , and SO_2 emitted from local transportation and regional industrial activities (Guo et al., 2014; Zhang et al., 2015).

Although the research conducted so far provided a lot of insights into the characteristics of haze aerosol PNSD, there have been basically no studies sufficiently focusing on the different stages of individual haze episodes, and in particularly on the mass concentration development stage. Lack of this fundamental information on PNSD is a factor limiting the understanding of Chinese haze and its corresponding contribution to optical, cloud, and global climate change. Therefore, in this study, real-time measurement campaigns were conducted to investigate the characteristics of PNSD using the Fast Mobility Particle Sizer (FMPS model 3091, TSI Inc.) in Xi'an urban atmosphere. The PNC, PNSD, their

temporal and diurnal variation, and NPF episodes were also investigated in detail. By comparing PNSD of submicron aerosols with other particle characteristics between normal days and haze episodes, as well as between different stages of haze episodes, we have gained better understanding of air pollution episodes in urban air.

Normal days are days when the 24-h average concentration of $\text{PM}_{2.5}$ is lower than the limit of $75 \mu\text{g m}^{-3}$ (Grade II of the NAAQS of China, GB 3095–2012), or the Individual Air Quality Index (IAQI) of $\text{PM}_{2.5}$ is lower than 100, which is classified as good air quality (HJ 633–2012). While these concentrations are higher than the World Health Organization guidelines of $25 \mu\text{g m}^{-3}$ for the 24-h average (WHO Regional Office for Europe, 2005), for simplicity we have referred to days with relatively low pollution conditions, which are normal in the winter in China, as “normal days” throughout the remainder of the paper.

2. Methodology

2.1. Sampling location

Xi'an is one of the largest cities in northwestern China, and has a sub-humid continental monsoon climate. It is also the center of politics, economy, culture and business for the local regions. Winters are cold with a little rain and snow, and with the average temperature of -0.5°C in January, while the extreme minimum temperature can be down to below -10°C under the impact of strong cold waves (<http://www.sxmb.gov.cn>).

Our monitoring was performed on the rooftop of a six-floor building located at Qujiang campus of Xi'an Jiaotong University (XJTU), approximately 20 m above the ground level, Fig. 1). The monitoring station was located 0.7 km away from a heavy trafficked road, and with no industrial source within the 1.5 km radius, to minimize the direct impact of traffic and industrial pollution.

2.2. Sampling methodology

The FMPS (TSI model 3091) was located at the selected location from December 9th, 2015 to January 8th, 2016 to monitor particles

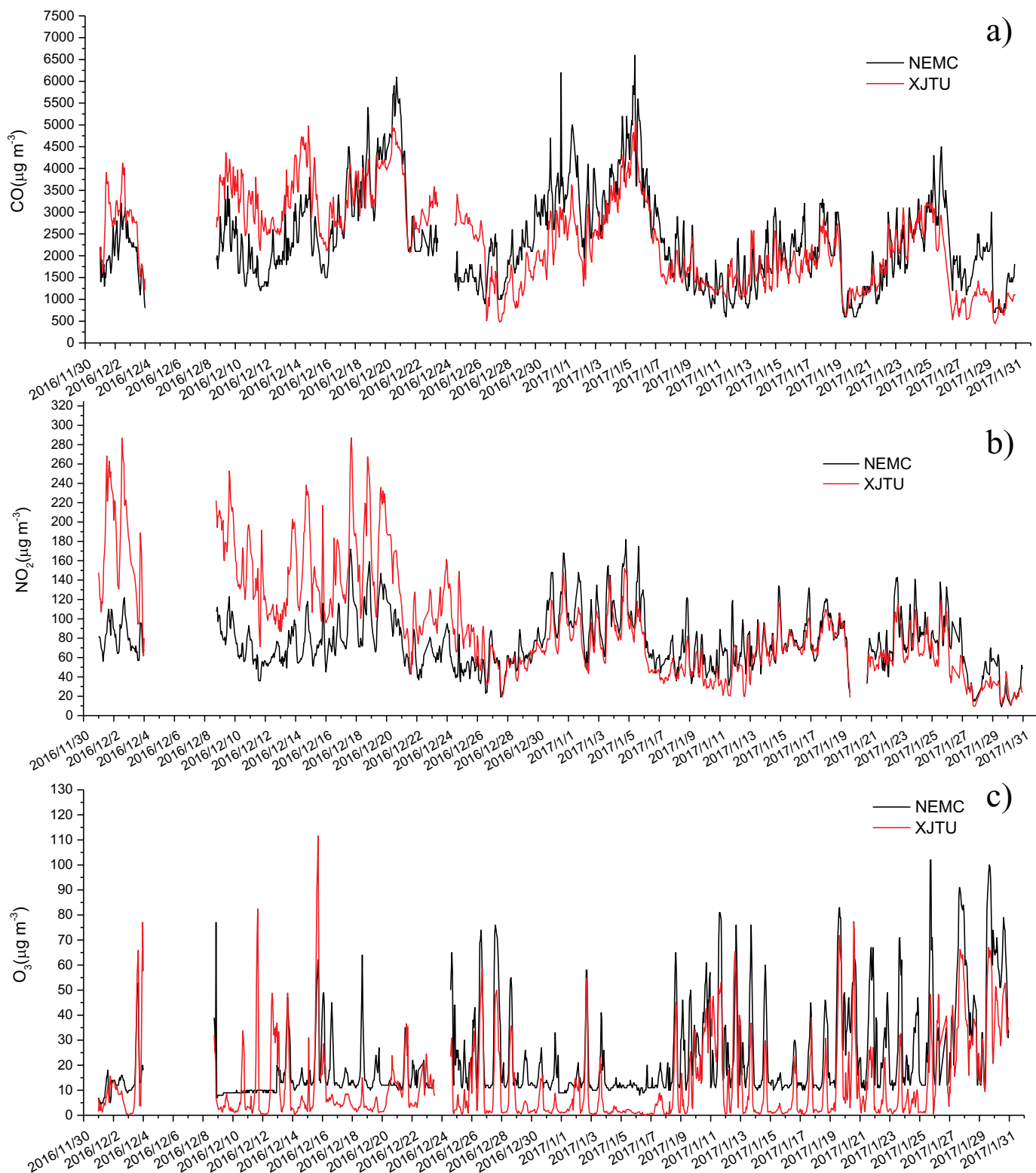


Fig. 2. A comparison of gaseous pollutants concentrations between the NEMC station and the XJTU stations.

with diameters within the 5.6 to 523 nm window. Based on the measured PNC, particle surface concentration (PSC) and particle volume concentration (PVC) were calculated by the FMPS. The FMPS has 32 size bins, the upper concentration range of $1 - 10^7 \text{ cm}^{-3}$, and the sampling frequency of the measurements was five minutes. To avoid potential contamination of dust resuspension, the inlet of the instrument was approximately 1.5 m above the ground of the rooftop.

Meteorological parameters (i.e., temperature, relative humidity (RH), wind speed (WS), and wind direction (WD)) were measured simultaneously at the same sampling site. $\text{PM}_{2.5}$ and gaseous pollutants (O_3 , SO_2 , NO_2 , CO) concentration data were obtained from the National Environmental Monitoring Centre (NEMC), 3.2 km away from the site. A comparison of gaseous pollutants (O_3 , NO_2 , CO) between the NEMC and XJTU stations was carried out from 1 December 2016 to 30 January

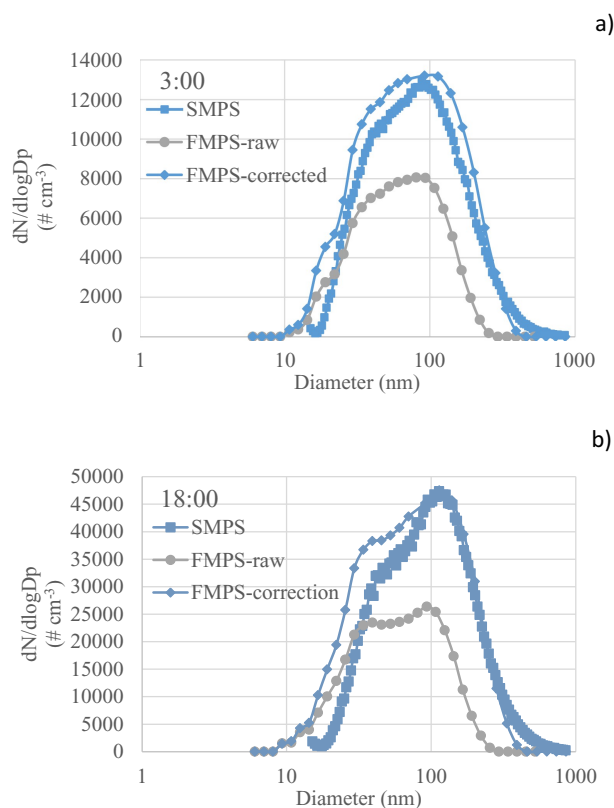


Fig. 3. Comparison of ambient particle size distribution measured simultaneously by the FMPS and SMPS at (a) 3:00 on 24 Dec 2015 and (b) 18:00 on 23 Dec 2015. Five-minute average number concentrations of ambient particles were used in this figure.

2017. Although there is a numerical difference on mass concentrations of gaseous pollutants such as O_3 , the temporal variation is similar for all pollutants (Fig. 2). The SO_2 data was not available because we did not have an SO_2 monitor at our station.

2.3. Correction of FMPS readings

The FMPS is a relatively recently developed instrument that offers an alternative electrostatic particle sizing method to the TSI Scanning Mobility Particle Sizer (SMPS) – considered here as the reference instrument. The SMPS has been proved to achieve more accurate PNC and PNSD (Zimmerman et al., 2015). When using an FMPS as a replacement for the SMPS it is important to first operate both instruments side by side to derive locally relevant correction factors (Lee et al., 2013).

To compare the SMPS with the FMPS in this study, PNC and PNSD were sampled from ambient air. The SMPS consisted of an electrostatic classifier (TSI model 3080), a differential mobility analyzer (DMA, TSI model 3081) and a butanol-based condensation particle counter (CPC, TSI model 3772). Five-minute average number concentrations of ambient particles measured by the two instruments were compared to derive correction factors of PNC readings by the FMPS. For the SMPS system, it is especially important to use multiple charge correction and diffusion loss correction when sizing aerosols smaller than 100 nm, because diffusion becomes increasingly important in this size range (Jeong and Evans, 2009). The correction is possible by choosing appropriate checkboxes in the system. After correction in the SMPS system, good correlation was found for the PNC_{100} between the SMPS and FMPS, with the correlation coefficient (R^2) equal to 0.86.

The data correction of FMPS in this study is a two-step protocol, which has been used by Zimmerman et al. (2015). The correction protocol consists of: (1) broadening the > 80 nm size range of the distribution to account for under-sizing by the FMPS based on Lee et al.' study (2013); and (2) applying an existing correction protocol in the 8–93 nm size range according to Jeong and Evans's study (2009).

Underestimation of the size of particles larger than 80 nm by the FMPS was reported in previous studies (Lee et al., 2013; Zimmerman et al., 2015). Lee et al. (2013) demonstrated that the FMPS significantly underestimated particle size, by 40–50%, which was established by comparing the particle sizing performance of an FMPS against simultaneous measurements with an Aerodyne Aerosol Mass Spectrometer (AMS), and an SMPS and sampling ambient particles in the size range of 50–450 nm. Using the slope and intercept from the linear least squares fit of the salt experiments, a simple correction algorithm for the FMPS size distribution was applied, which significantly reduced the discrepancy with respect to the SMPS and AMS measurements. The effectiveness of this correction was further proved to be capable of considerably reducing the initial sizing discrepancy for urban ambient air by Zimmerman et al. (2015). Zimmerman et al. (2015) published the adjusted size bins for particles larger than 80 nm by FMPS, as shown in Table 2 in their paper. The adjusted size bin = (original size bin-25)/0.58. Uncertainty is calculated based on the standard deviations on the regression slope and intercept. Thus, the size bin diameter in this study was broadened based on previous studies in order to reduce the sizing discrepancy.

The total PNC measured by FMPS and SMPS agreed well, with the correlation coefficient equal to 0.85. However, the PNC measured by the SMPS was on average 1.7 times that of the FMPS. The discrepancies in particle counting have been reported in previous studies (Asbach et al., 2009; Lee et al., 2013; Jeong and Evans, 2009; Zimmerman et al., 2015). PNC in the size range of 8–93 nm was significantly underestimated by the FMPS and needed to be corrected (Jeong and Evans, 2009). Therefore, in our study, the FMPS-measured PNC of each particle size bin from 8 nm to 93 nm was multiplied by the ratio of total PNC_{SMPS}/PNC_{FMPS} as the second step of the data processing.

An adequate accuracy of the particle size measurements was achieved after the above two-step correction, as shown in Fig. 3. The observations suggest that it is crucial to evaluate the sizing performance of the FMPS against other instruments to ensure an adequate accuracy of the particle size measurements.

2.4. Data analysis

Pollution process analysis was applied in the current study. We linked a series of $PM_{2.5}$ observations and then filtered out pollution processes based on two criteria of the average mass concentration of $PM_{2.5}$ over $250 \mu g m^{-3}$ and duration time equal to or > 3 h. This is in accordance with the severely polluted Air Quality Index (AQI) level (AQI > 300) published by the Ministry of Environmental Protection of the People's Republic of China (China, 2012). Two kinds of pollution processes were studied: with rapid $PM_{2.5}$ concentration growth (e.g., short-term episodes) and with persistent growth (e.g., prolonged hazes). $PM_{2.5}$ concentration growth rate in a short-term episode was defined as higher than $10 \mu g m^{-3} h^{-1}$, which is the upper limit of sulfate production rate in a rapid record-breaking pollution process in Beijing in January 2013 (Cheng et al., 2016). Then, pollution process analysis was used during haze episodes: characteristics of $PM_{2.5}$, gaseous pollutants, PNC, PNSD, and meteorological variables were identified by comparing those parameters with normal days, and between different stages of haze episodes. $PM_{2.5}$ pollution formation mechanisms were explored by evaluating pollution strength (growth rates) in relation to $PM_{2.5}$, gaseous pollutants, PNC, PNSD, and meteorological variables in these processes. Our results were compared with those from previous studies. SPSS Statistics software was used to perform statistical analysis in this study.

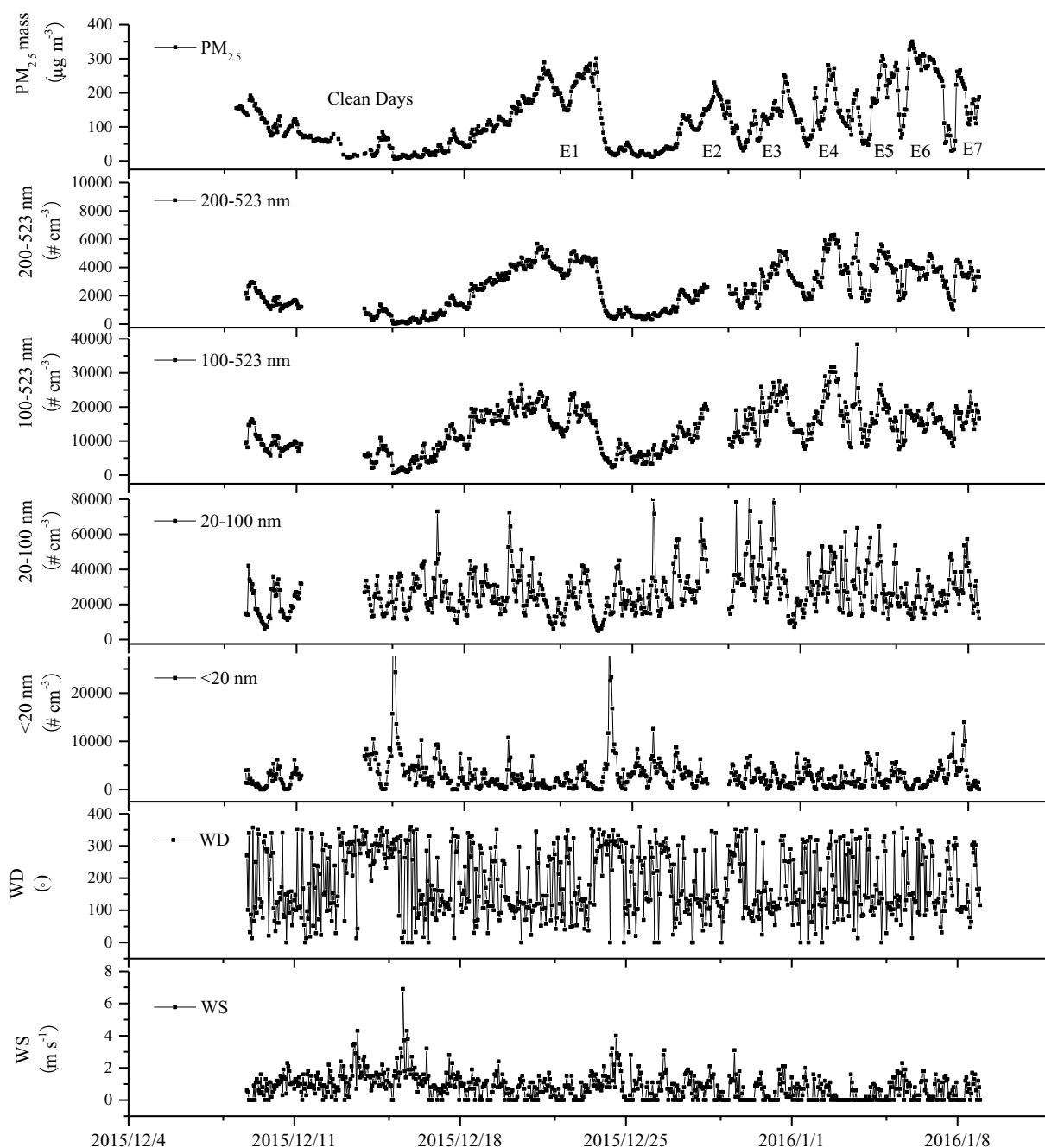


Fig. 4. The temporal variation of $PM_{2.5}$, particle number concentration, wind direction (WD), and wind speed (WS) in different modes during the observation period.

3. Results and discussions

3.1. Temporal variation of particulate mass and number

The temporal variation of $PM_{2.5}$ concentrations revealed seven haze episodes during the sampling campaign, including a nine-day one (E1) lasting from 15 to 24 Dec. 2015 and six two-day severe episodes (E2–E7, occurring every three days) during the period from 30 Dec. 2015 to 7 Jan. 2016 (Fig. 4). E1 and E6 were comprehensively investigated in this study because E1 was the only prolonged haze episode with a low growth rate of $2 \mu\text{g m}^{-3} \text{h}^{-1}$ at the increase phase, and E6 was a good representative of all short-term episodes with an average high growth rate of $13 \mu\text{g m}^{-3} \text{h}^{-1}$, as shown in Fig. 4.

The average concentrations of PM_{10} and $PM_{2.5}$ on normal days

(11–14 Dec) were $131 \mu\text{g m}^{-3}$ and $50 \mu\text{g m}^{-3}$, respectively (Table 1), while during E1, $245 \mu\text{g m}^{-3}$ and $118 \mu\text{g m}^{-3}$, which was 87% and 137% higher, respectively than on normal days. The average concentrations of PM_{10} and $PM_{2.5}$ during E6 were $474 \mu\text{g m}^{-3}$ and $260 \mu\text{g m}^{-3}$, which were 263% and 424% higher than those measured on normal days. The ratio of $PM_{2.5}/PM_{10}$ changed from 0.38 on normal days to 0.47 and 0.55 during E1 and E6, respectively, which suggests that the increment of $PM_{2.5}$ was more significant than that of PM_{10} during haze episodes. In addition, as it can be seen from Fig. 4, north wind always brings relatively clean air to the Xi'an city, while east or low speed wind leads to haze events. The pattern can be clearly seen on the example of E1: north wind was prevailing before and after E1. It is also true for E2 to E7, but the north wind lasted for only a couple of hours in between these episodes. The days with the highest particle

Table 1

Descriptive statistics of particle characteristics, gaseous species concentrations and meteorological parameters for the entire study, before and during the haze episodes, and the percentage changes during the haze episodes.

	Entire study	Clean days	E1	Change (%) of E1& Clean days ^a	E6	Change (%) of E6& Clean days ^a
Meteorological parameters						
T (°C)	3 (−6–13)	4 (−2–13)	2 (−6–9)	−1	1 (−2–5)	−1
RH (%)	61 (17–91)	55 (17–86)	53 (18–81)	0	76 (54–90)	0
PM & gaseous species ($\mu\text{g cm}^{-3}$)						
PM ₁₀	257 (43–687)	131 (43–303)	245 (47–591)	87%	474 (143–687)	263%
PM _{2.5}	122 (6–351)	50 (6–134)	118 (36–300)	137%	260 (52–351)	424%
NO ₂	102 (26–318)	72 (26–111)	102 (26–177)	41%	134 (48–194)	85%
SO ₂	57 (15–185)	41 (15–78)	67 (15–185)	62%	48 (29–89)	17%
O ₃	21 (16–68)	16 (16–17)	23 (16–68)	41%	20 (16–39)	22%
Particle number, surface & volume concentrations						
Nucleation (N_{20} , $\times 10^4 \text{ cm}^{-3}$)	0.31 (0.0019–4.30)	0.42 (0.0044–1.05)	0.35 (0.0012–4.30)	−16%	0.19 (0.0019–0.59)	−54%
Aitken (N_{20-100} , $\times 10^4 \text{ cm}^{-3}$)	2.75 (0.49–9.05)	2.24 (1.12–3.64)	2.52 (0.49–7.30)	12%	2.21 (1.17–3.96)	−2%
Accumulation ($N_{100-523}$, $\times 10^4 \text{ cm}^{-3}$)	1.36 (0.061–8.46)	0.70 (0.21–0.99)	1.31 (0.061–2.66)	88%	1.60 (0.89–2.10)	130%
Total PNC ($\times 10^4$, cm^{-3})	4.37 (1.32–11.73)	3.35 (1.92–4.75)	4.14 (1.42–9.93)	23%	3.99 (2.54–6.06)	19%
Total PSC ($\times 10^8 \text{ nm}^2 \text{ cm}^{-3}$)	7.73 (0.73–20.70)	4.17 (1.45–5.77)	7.52 (0.73–15.20)	80%	9.24 (5.59–12.10)	121%
Total PVC ($\times 10^{10} \text{ nm}^3 \text{ cm}^{-3}$)	1.92 (0.09–5.00)	0.92 (0.27–1.36)	1.91 (0.09–3.77)	107%	2.52 (1.38–3.28)	173%

^a Calculation of change of pollution between episode & clean days: $(C_{\text{episode}} - C_{\text{clean}}) \times 100 / C_{\text{clean}}$.

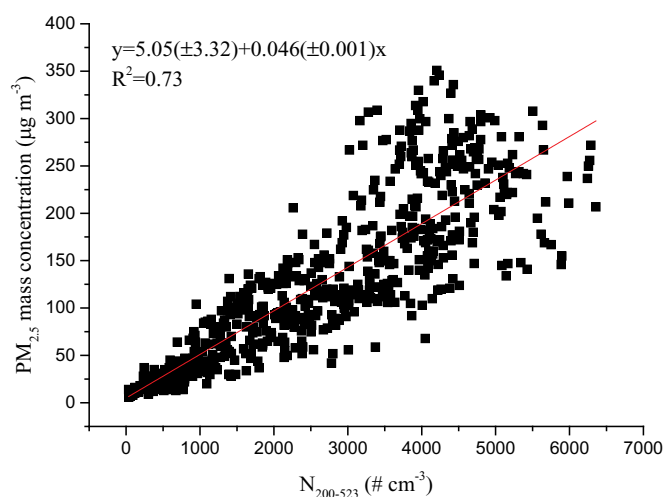


Fig. 5. Comparison between PM_{2.5} and N_{200–523} particle number concentrations.

concentrations during the observation period were all found to be during haze episodes, with east or low speed wind prevailing. The days with the lowest particle concentrations were during normal days with prevailing north wind (Fig. 4).

For the analysis, the 5.6–523 nm PNC size range was divided into four size ranges: (i) smaller than 20 nm (N_{20}), (ii) 20–100 nm (N_{20-100}), (iii) 100–523 nm ($N_{100-523}$), and (iv) 200–523 nm ($N_{200-523}$). Similar to a previous study by Peng et al. (2014), we used the former three size ranges to represent the modes of nucleation, Aitken, and accumulation. The largest size range was also in the accumulation mode, but only including particles larger than 200 nm. The temporal variation of PM_{2.5} concentrations and the PNC of nucleation/Aitken mode particles were significantly different, indicating that the particles belonging to these three ranges originated from different sources. Examining the temporal variations of PNC, it can be seen that the variations of $N_{100-523}$ and $N_{200-523}$ were similar to the trend of PM_{2.5} concentrations (Fig. 4). The correlation coefficient (R^2) between PM_{2.5} and $N_{200-523}$ is 0.73 (Fig. 5), which is higher than between PM_{2.5} and $N_{100-523}$ (0.48), indicating that the particles with diameters within $N_{200-523}$ made large contributions to the PM_{2.5} concentrations.

3.2. Comparison of particle number concentrations between normal days and haze episodes

Descriptive statistics of PNC in the nucleation, Aitken, and accumulation modes are shown in Table 1. The average total PNC values were $3.35 \times 10^4 \text{ cm}^{-3}$, $4.14 \times 10^4 \text{ cm}^{-3}$, and $3.99 \times 10^4 \text{ cm}^{-3}$ during normal days, E1, and E6, respectively, showing a statically significant increase in PNC from normal days to haze days ($p = .000$ for E1 and $p = .002$ for E6, two-tailed t-test). Average PNC in nucleation, Aitken, and accumulation modes on normal days were $0.42 \times 10^4 \text{ cm}^{-3}$, $2.24 \times 10^4 \text{ cm}^{-3}$, and $0.70 \times 10^4 \text{ cm}^{-3}$, respectively. Compared with the PNC during normal days, clear increases in the accumulation mode (88% for E1 and 130% for E6) were found during haze episodes with a statistically significant difference ($p = .000$ for E1 and $p = .000$ for E6, two-tailed t-test). The ratio of PNC in accumulation mode / total PNC changed from 0.21 during normal days to 0.32 during E1 and 0.40 during E6, which demonstrates a relative increase in the concentration of the accumulation mode particles during haze episodes. In contrast, compared with normal days, the changes in PNC during E1 were not statistically significant in the nucleation ($p = .478$) and Aitken modes ($p = .069$), while the changes in the nucleation mode ($p = .000$) were statistically significant during E6. A decrease of approximately 54% in PNC in the nucleation mode was observed during E6, but the decrease was only ~16% during E1. The ratio of PNC in the nucleation mode to the total PNC also decreased from 0.13 during normal days to 0.05 during E6 (and to 0.09 during E1). Thus, PNC in the accumulation mode significantly increased, but in the nucleation mode, PNC decreased during E6, which is not the case for E1.

The PSC during normal days, E1, and E6 were $4.17 \times 10^8 \mu\text{m}^2 \text{ cm}^{-3}$, $7.52 \times 10^8 \mu\text{m}^2 \text{ cm}^{-3}$, and $9.24 \times 10^{10} \text{ nm}^2 \text{ cm}^{-3}$, respectively. Clear increases in PSC were seen during haze episodes (80% for E1 and 121% for E6). With the increase in PSC, as expected, the increases in PVC were even larger – 107% and 173% for E1 and E6, respectively.

3.3. Comparison of diurnal variation in PNSDs between normal days and haze episodes

The diurnal PNSD patterns during clean and haze days were investigated separately and are presented in Fig. 6. The PNSD was bimodal during normal days, with the main peak centered at 139 nm (computed based on a normal distribution) at 0:00 am, at 168 nm at 4:00 am and at 60–70 nm during daytime. The larger particle size at night was associated with particle age and growth under high RH,

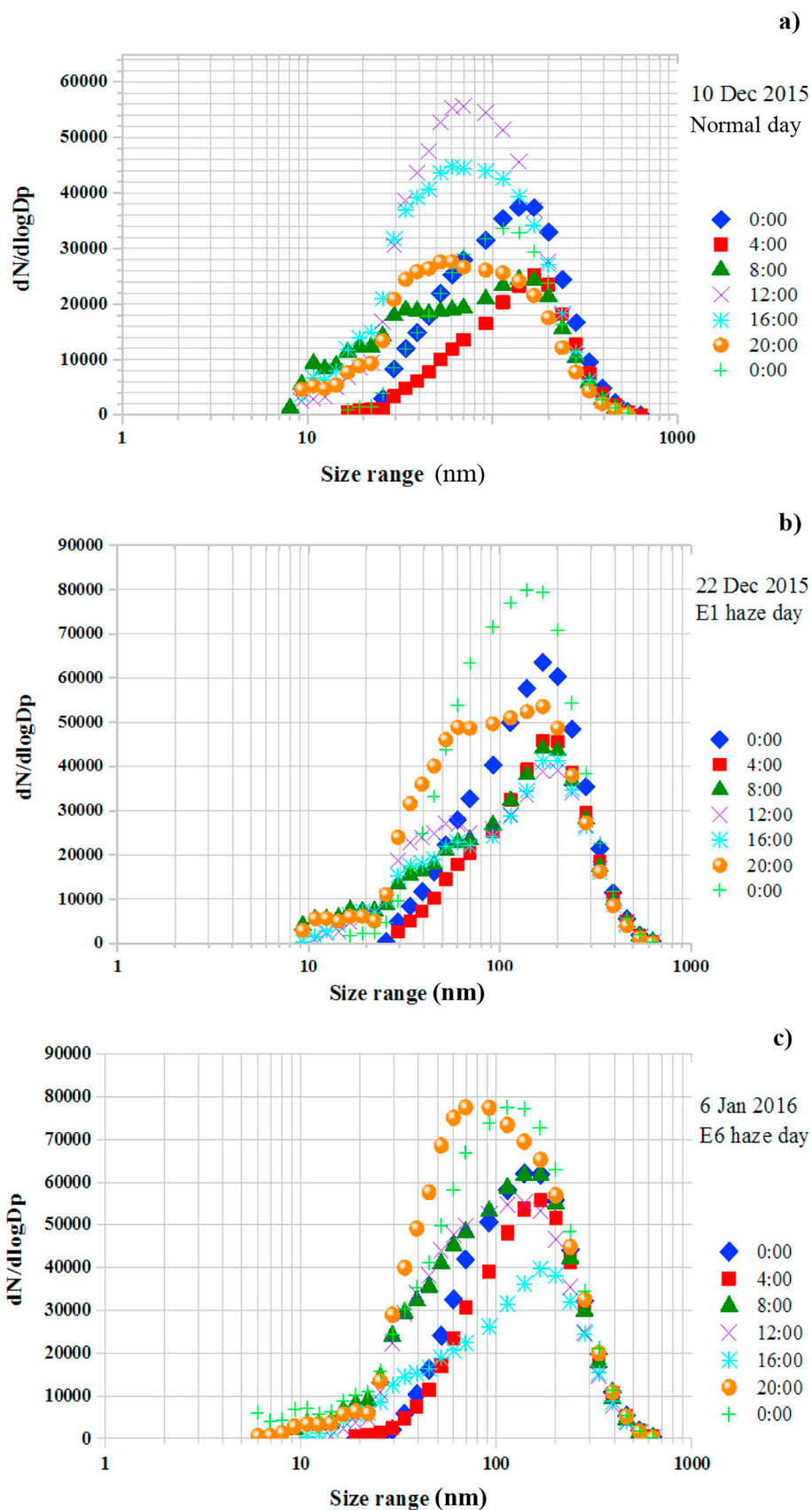
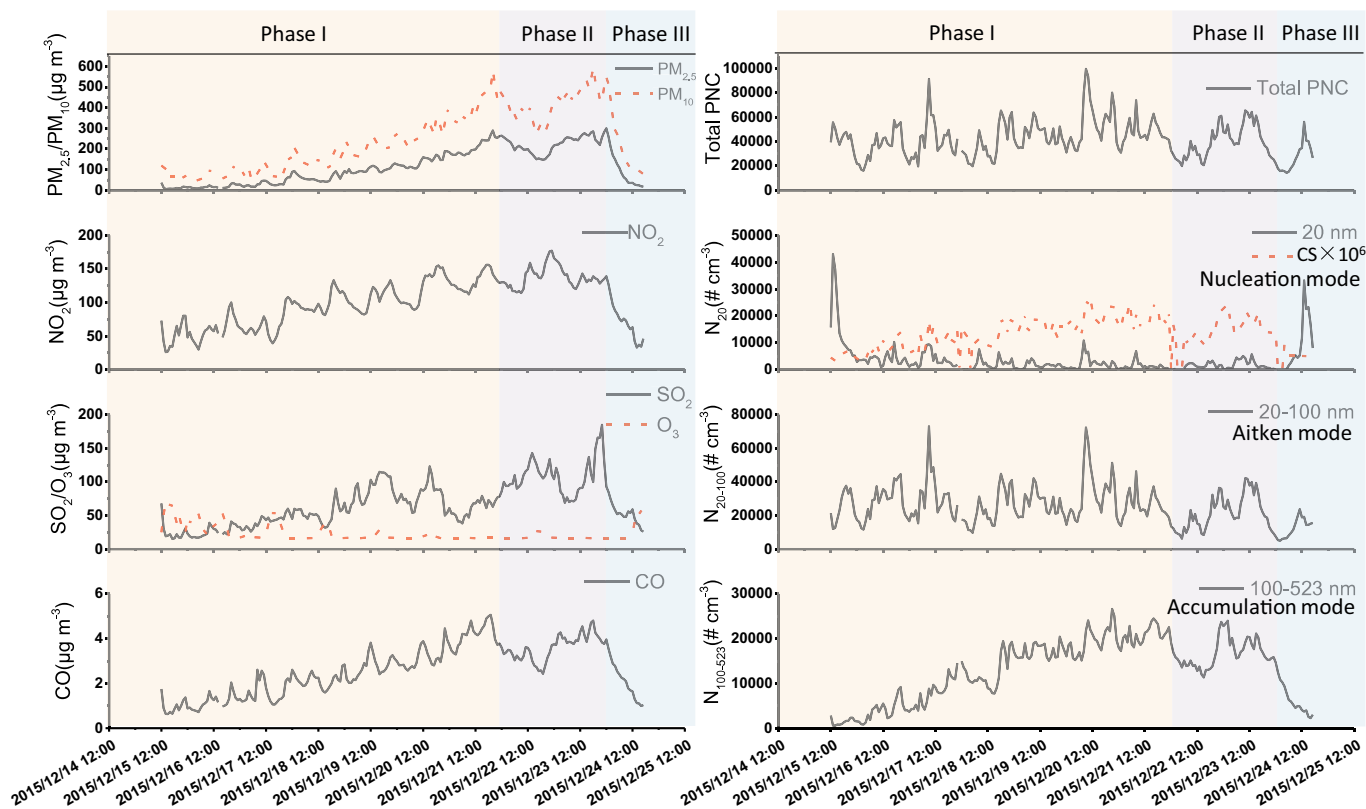


Fig. 6. Size distribution of particle number concentration during normal day on (a) 10 Dec 2015 and haze days on (b) 22 Dec 2015 and (c) 6 Jan 2016.

a) E1



b) E6

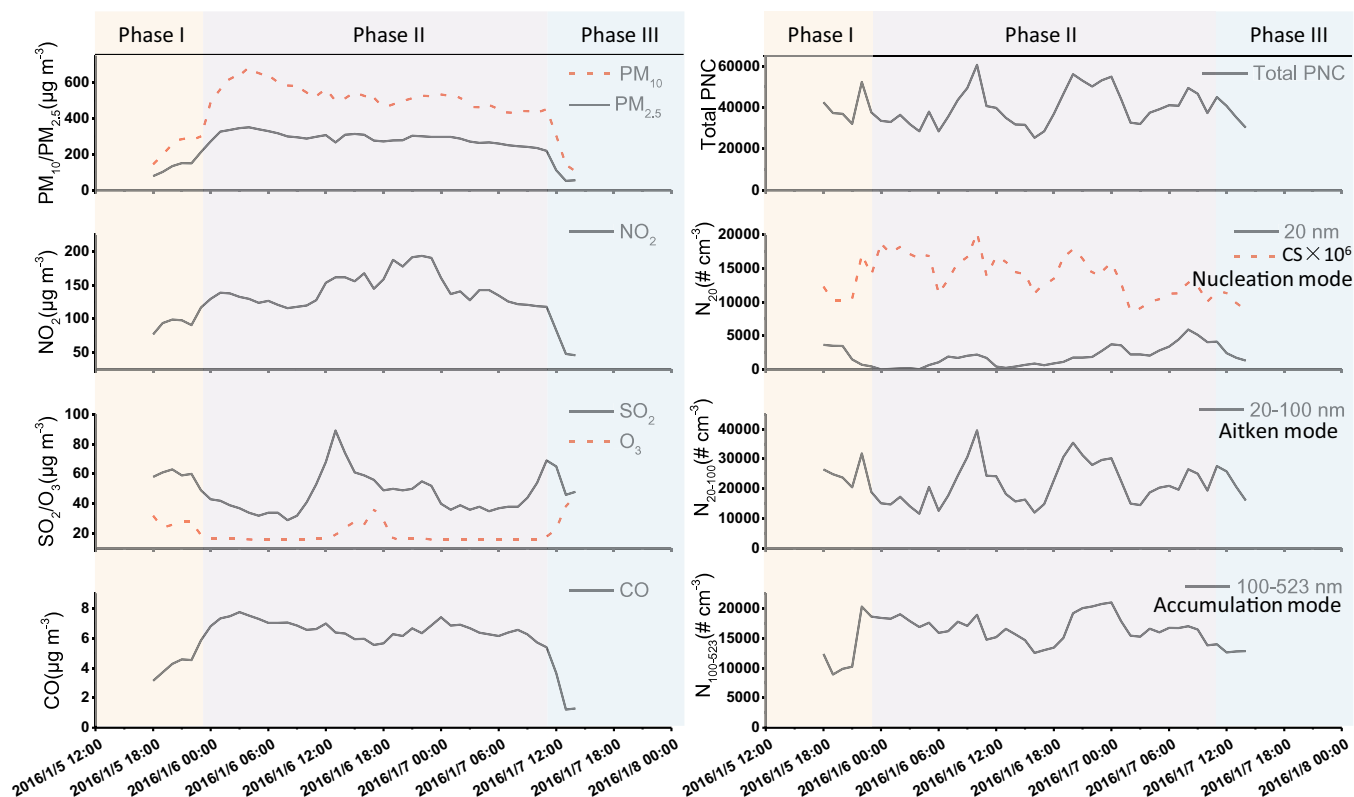


Fig. 7. Evolution characteristics of the haze episodes of (a) E1 and (b) E2. We calculated the condensation sink using the method described by Pirjola et al. (1998) and Kulmala et al. (2001).

Table 2
Evolution characteristics of the haze episodes.

	Phase I (haze develops)	Phase II (high particle pollution)	Phase III (rapid decrease)
E1			
Meteorological parameters			
T (°C)	1 (–6–7)	3 (2–6)	5 (3–9)
RH (%)	50 (18–81)	59 (40–70)	56 (26–73)
PM & gaseous species ($\mu\text{g cm}^{-3}$)			
PM ₁₀	194 (47–578)	410 (274–540)	290 (78–591)
PM _{2.5}	88 (36–289)	218 (148–280)	136 (18–300)
NO ₂	94 (26–156)	139 (114–177)	89 (33–139)
SO ₂	56 (15–123)	103 (69–143)	78 (26–185)
O ₃	24 (16–68)	18 (16–27)	24 (16–59)
CO	2 (1–5)	4 (2–5)	3 (1–5)
PM _{2.5} growth rate	37–262 (155 h)	264–280 (41 h)	285–18 (13h)
Particle number, surface & volume concentrations			
Nucleation (N ₂₀ , $\times 10^4 \text{ cm}^{-3}$)	0.35 (0.0012–4.30)	0.19 (0.0057–0.57)	0.68 (0.0022–3.32)
Aitken (N _{20–100} , $\times 10^4 \text{ cm}^{-3}$)	2.78 (0.96–7.31)	2.24 (0.63–4.22)	1.31 (0.49–2.37)
Accumulation (N _{100–523} , $\times 10^4 \text{ cm}^{-3}$)	1.27 (0.06–2.66)	1.69 (1.13–2.40)	0.88 (0.23–1.70)
Total PNC ($\times 10^4 \text{ cm}^{-3}$)	4.37 (1.61–9.93)	4.08 (1.98–6.54)	2.78 (1.42–5.61)
Total PSC ($\times 10^8 \text{ nm}^2 \text{ cm}^{-3}$)	7.24 (0.72–15.20)	9.87 (0.73–13.50)	5.25 (1.56–10.00)
Total PVC ($\times 10^{10} \text{ nm}^3 \text{ cm}^{-3}$)	1.74 (0.087–3.77)	2.76 (1.93–3.50)	1.48 (0.31–2.85)
E6			
Meteorological parameters			
T (°C)	3 (1–4)	1 (–2–5)	4 (4–5)
RH (%)	66 (56–79)	78 (59–90)	57 (54–61)
PM & Gaseous species ($\mu\text{g cm}^{-3}$)			
PM ₁₀	249 (144–296)	526 (429–687)	184 (106–304)
PM _{2.5}	138 (79–213)	290 (219–351)	73 (52–111)
NO ₂	96 (77–117)	144 (116–194)	59 (46–83)
SO ₂	58 (49–63)	46 (29–89)	53 (46–65)
O ₃	26 (19–32)	18 (16–37)	35 (23–44)
CO	4 (3–6)	7 (5–8)	2 (1–4)
PM _{2.5} growth rate	79–213 (5 h)	272–219 (35 h)	111–56 (4 h)
Particle number, surface & volume concentrations			
Nucleation (N ₂₀ , $\times 10^4 \text{ cm}^{-3}$)	0.22 (0.04–0.37)	0.19 (0.00019–0.59)	0.18 (0.13–0.24)
Aitken (N _{20–100} , $\times 10^4 \text{ cm}^{-3}$)	2.44 (1.90–3.18)	2.18 (1.17–3.96)	2.09 (1.61–2.58)
Accumulation (N _{100–523} , $\times 10^4 \text{ cm}^{-3}$)	1.34 (0.89–2.03)	1.67 (1.25–2.10)	1.27 (1.26–1.28)
Total PNC ($\times 10^4 \text{ cm}^{-3}$)	3.98 (3.21–5.23)	4.02 (2.54–6.06)	3.54 (3.03–4.08)
Total PSC ($\times 10^8 \text{ nm}^2 \text{ cm}^{-3}$)	7.90 (5.59–11.60)	9.61 (7.20–12.10)	7.42 (7.36–7.48)
Total PVC ($\times 10^{10} \text{ nm}^3 \text{ cm}^{-3}$)	2.06 (1.38–2.99)	2.64 (2.10–3.28)	1.96 (1.91–2.02)

which was over 80% at 0:00 are, and over 90% at 4:00 am, the highest diurnal RH. The smaller size during daytime was due to fresh emissions, which also generated the second minor peak centered at 39 nm. The highest PNC during daytime was around 12:00 noon, arising from combined effect of fresh emission from various anthropogenic emissions. Subsequently, the PNC kept gradually decreasing through the afternoon until evening.

The diurnal variation of PNSD during E1 and E6 episodes was less pronounced than on the normal days, with the centers of the main peaks located within larger size ranges, at 179 nm for E1 and 137 nm for E6 for the daily averaged data. When considering diurnal variation in the peak locations, the minima were at night, at 168 nm at 0:00 am and 4:00 am for E1 and 70 nm at 8:00 pm for E6. The highest PNC were seen at night (e.g. 20:00 pm, 0:00 am), which is opposite to normal days, which we hypothesize to be due to stagnant meteorological conditions that suppress air dispersion during the haze episodes.

3.4. Evolution of haze characteristics

As discussed above, the three phases of haze in relation to PM_{2.5} concentration include an increase (Phase I); relatively stable and high for hours/days (Phase II); and rapid decrease (Phase III). Fig. 7 and Table 2 present the evolution characteristics of pollutants during three phases of E1 and E6. During both episodes, the average PM₁₀ and PM_{2.5} concentrations in Phase II were more than twice as high as the concentrations in Phases I and III. However, the variation of PM_{2.5} concentrations during Phases I and III were much more significant than during Phase II, as indicated by the ranges between the minima and the maxima. Thus, the prolonged haze episode, represented by E1, is characterized by a long-duration Phase I of 115 h, with sustained increase of PM_{2.5} at a low growth rate of $2 \mu\text{g m}^{-3}$ per hour, and the increase of PM_{2.5} concentration from 37 to $262 \mu\text{g m}^{-3}$, during this period. The short-term episodes, including E2–E7 and represented by E6, characterized by a short-duration Phase I (5 h) with a rapid increase of PM_{2.5} at a high growth rate of $27 \mu\text{g m}^{-3}$ per hour and PM_{2.5} from 79 to $213 \mu\text{g m}^{-3}$.

E1 started and ended with an NPF episode (Fig. 7a) during the relatively clean period, along with higher wind speeds (averaging $4.1 \pm 1.9 \text{ m s}^{-1}$ and $2.6 \pm 1.0 \text{ m s}^{-1}$) compared with the stagnant air mass (averaging $0.9 \pm 0.7 \text{ m s}^{-1}$) during the remaining period of E1. During E1, the total, the nucleation mode, and the Aitken mode PNC were all reduced from phase I to III, but the accumulation mode PNC increased during phase II (Table 2). This indicated continuous growth from the nucleation mode particles by the evolution in the particle size (Fig. 7a). Concentrations of SO₂ and NO_x slowly elevated during the same period when PM_{2.5} gradually increased (Fig. 7a). As well as the increase in mass, NO_x and CO had daily cycles (Fig. 7a), showing the effects of local sources of traffic emissions and coal combustion for heating purposes, respectively. All characteristics of E1 are consistent with the 4–7 d periodic cycle of PM episodes in Beijing as described by Guo et al. (2014). These episodes are governed by meteorological conditions and characterized by the two distinct aerosol formation processes of nucleation and growth. Nucleation produces high particle number concentrations at the beginning of a pollution cycle, and the photochemical oxidation of volatile organic compounds (VOCs) and NO_x from urban traffic emissions and SO₂ from regional industrial sources are primarily responsible for the sustained growth from the nucleation mode particles over multiple days (Guo et al., 2014).

During E6, the total PNC showed a different pattern to that of particle mass, which was, on average, a downward trend from phase I to II and III (Table 2). Similar to E1, clear decreases in the PNC of the nucleation and Aitken modes were observed between Phases I and II, but there was a clear increase in the accumulation mode PNC. This indicates that particle size distribution shifted to large particles as haze developed. However, no NPF episodes were observed at the beginning and the end of E6 (Fig. 7b). Compared with the NPF episodes during E1, phase I of E6 showed relatively polluted conditions, with a higher PM_{2.5} mass concentration ($138 \mu\text{g m}^{-3}$) and lower wind speed ($0.9 \pm 0.6 \text{ m s}^{-1}$). Nucleation mode particles formed through the condensation process of supersaturated gases. The nucleating molecules have to cluster faster to avoid being lost onto the surface of pre-existing particles, which is the most important sink for nucleating molecules and is defined as a condensation sink (CS). The CS for condensable gases has a preventing influence on nucleation and subsequent growth (Kulmala et al., 2001). Fig. 7 shows the CS in the three phases for both E1 and E6. The average CS during E6 was $1.24 \times 10^{-2} \pm 2.8 \times 10^{-3}$, $1.4 \times 10^{-2} \pm 3.0 \times 10^{-3}$, $1.0 \times 10^{-2} \pm 1.3 \times 10^{-3}$ for phase I, II, and III, respectively – about 2–3 times of that during the NPF episodes of E1 ($3.7 \times 10^{-3} \pm 5.9 \times 10^{-4}$ and $4.8 \times 10^{-3} \pm 6.0 \times 10^{-4}$). The higher the CS, the more rapidly gas molecules are scavenged by condensation onto pre-existing particles. This explains the absence of NPF episodes during E6. Nucleation is typically completely suppressed when the aerosol surface area exceeds $100 \mu\text{m}^2 \text{ cm}^{-3}$ (Aalto et al., 2001).

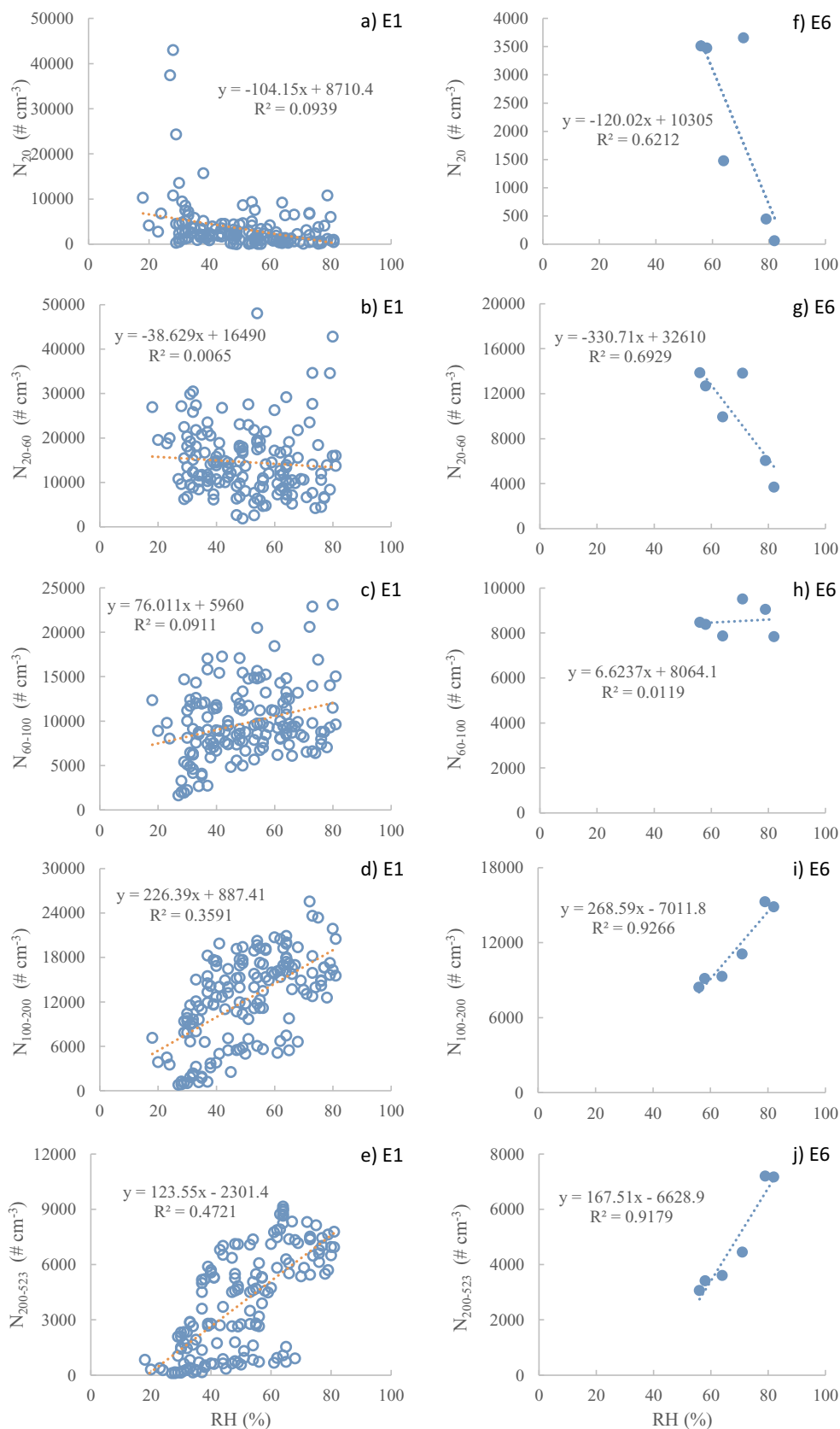


Fig. 8. Correlations between PNC and RH during Phase I of E1 (a-e) and E6 (f-j).

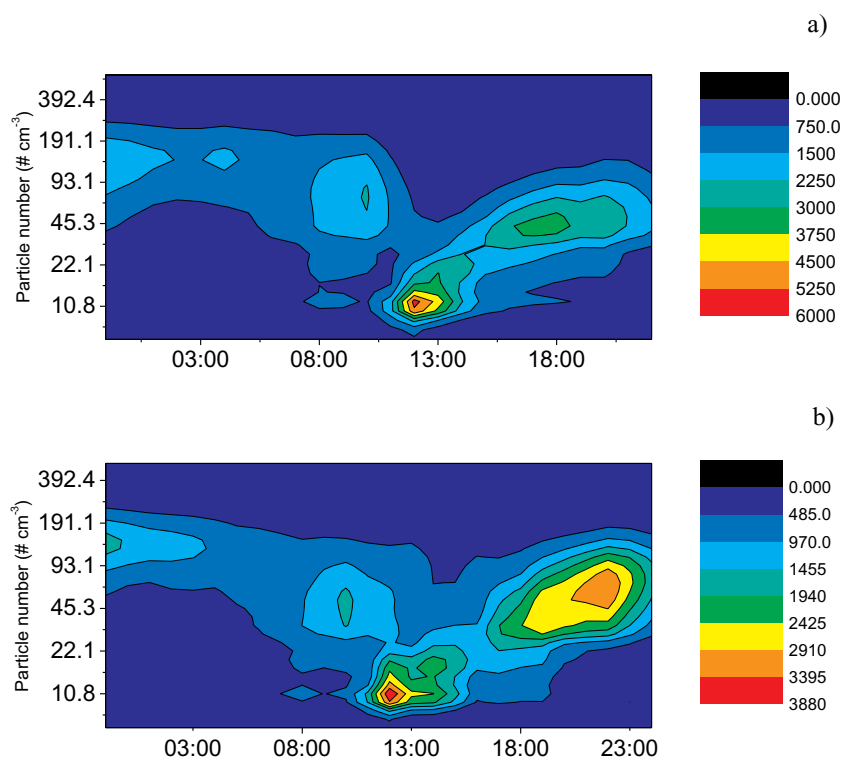


Fig. 9. Diurnal variation of PNC on (a) 15 Dec 2015 and (b) 24 Dec 2015.

In this study, the PSC concentration during E6 had exceeded the critical limits of $100 \mu\text{m}^2 \text{cm}^3$. Thus new particle formation was typically completely suppressed, which is consistent with our previous results from the CS.

The concentrations of NO_2 and CO showed similar trends to $\text{PM}_{2.5}$ concentrations during E6, with the highest values during phase II and a rapid decrease during phase III. By contrast, SO_2 showed a decreasing trend from $60 \mu\text{g m}^{-3}$ to $29 \mu\text{g m}^{-3}$ within 12 h, starting from the point when $\text{PM}_{2.5}$ and relative humidity (RH) started to increase during phase I. Concerning the high NO_2 and SO_2 concentrations, the reduction of SO_2 is likely transferred to sulfate on particle surfaces by aqueous oxidation of SO_2 by NO_2 (Wang et al., 2016), which has been proved to reach a high reactive rate within a couple of hours. The relatively high RH range of 56–79 during phase I also favored the transformation according to Wang et al. (2016). Laboratory work has proved that aqueous SO_2 oxidation by NO_2 is favored on fine aerosols with a air condition of a high RH (> 60–70%) and sufficient neutralization ($\text{pH} = 7$), which is the case for the rapid increases in $\text{PM}_{2.5}$ during haze episodes in China (Wang et al., 2016).

3.5. Impact of RH on PNC as haze develops in phase I

Since the changes of pollutant physical and chemical properties are most significant during Phase I, the correlation between PNC and RH was examined during Phase I of E1 and E6, as shown in Fig. 8. RH was in the range from 18 to 81% and from 54% to 90% during E1 and E6, respectively. Except for N_{60-100} , good correlation between PNC and RH was found for particles of all size ranges during E6, with correlation coefficients (R^2) of 0.62–0.92. The nucleation and the Aitken modes PNC (N_{20} and N_{20-60}) decreased as of RH increased from 54% to 90%, while PNC of accumulation modes ($N_{100-200}$ and $N_{200-523}$) increased. Deposition is apparently not the reason of the decrease in the nucleation or the Aitken mode PNC since the deposition rate is low for particles with diameter < 70 nm (Wang et al., 2017b), however RH plays a sizable role in particle coagulation (Wang et al., 2017). Water vapor

markedly decreases the stability of particles when RH exceeds 55%, which leads to efficient coagulation of particles (Hayakawa, 1964). Thus the decrease in the nucleation and the Aitken modes PNC was attributed to effective coagulation with preexisting particles, leading to the increase in accumulation mode particles at the same time.

Examining correlations during E1, it was found that they were not as clear as those during E6. The correlation coefficients (R^2) between RH and PNC are poor, of 0.094, 0.0065, 0.091 for N_{20} , N_{20-60} , and N_{60-523} , respectively. A somewhat better positive correlation is for $N_{100-200}$ and $N_{200-523}$, ($R^2 = 0.36$ and 0.47, respectively), suggesting that there was a certain degree of particle coagulation as RH increased, however, it is not as obvious as in E6. This is likely attributed to the impact of primary particle emissions and planetary boundary layer (PBL) variations, because the total PNC, PNC in nucleation, and Aitken mode showed a clear daily cycle, with high concentrations during daytime and low concentrations during nighttime (Fig. 7a).

3.6. New particle formation

NPF episodes are typically identified based on three criteria (Birmili and Wiedensohler, 2000). First, a sudden increase in PNC in the nucleation mode should occur. Second, the concentration of primary species, such as black carbon, should not increase significantly. Third, the episodes should last for > 2 h. The criteria were applied and tested in this study. NPF episodes usually occur during daytime when the pre-existing particle mass concentration is low and under sunny and dry conditions (Birmili and Wiedensohler, 2000; Stanier et al., 2004).

Only two NPF episodes were observed, on 15 and 24 December 2015, and Fig. 9 presents the two cases, with the superficial area of particle accumulation mode. The NPF episode occurred approximately at noon, with a burst of PNC in the nucleation mode, and continued increase in the size of the particles. As illustrated in Fig. 9, PNC with diameters < 20 nm exhibited extremely high concentrations at noon, indicating a burst of nucleation mode particles, followed by a clear growth process. The particle-phase sulfate can be formed during the

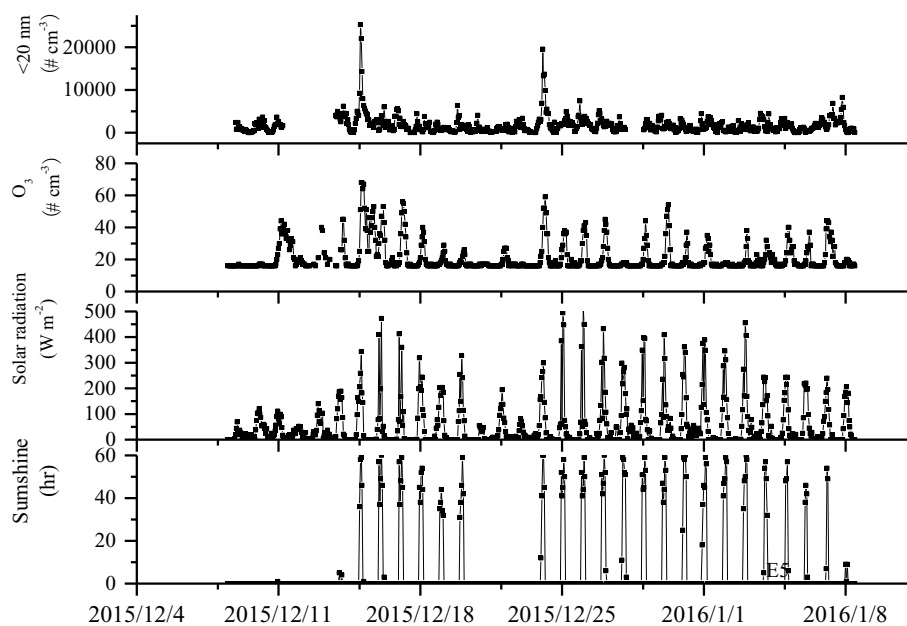


Fig. 10. The concentration of O₃, particles with diameters below 20 nm, solar radiation and sunshine hours during the observation period.

NPF episodes as a result of high atmospheric concentrations of SO₂, exceeding 40 ppbv (Guo et al., 2014). Our measurements showed simultaneous peaks of solar radiation, sunshine hours, and O₃ (Fig. 10), which support increased photo-chemical reactions in the atmosphere. The concentration of PM_{2.5} and CS were lower when the NPF episodes occurred (Fig. 7), suggesting a weak sink for the nucleation mode particles and precursors.

4. Conclusion

Deteriorating air quality in China has created global interests in haze's formation mechanism. In this study we report on the characteristics of PNSD in winter in Xi'an, to contribute towards better understanding of Chinese haze and its drivers. Compared to normal days, the average concentrations of PM₁₀ and PM_{2.5} increased from 131 μg m⁻³ and 50 μg m⁻³ to 245 μg m⁻³ and 118 μg m⁻³ during E1 (87% and 137%, respectively), and to 474 μg m⁻³ and 260 μg m⁻³ during E6 (263% and 424%, respectively). We found an increase in the proportion of accumulation mode particle concentration during haze episodes, with the number concentration ratio of the accumulation mode particles to the total particles changing from 0.21 on relatively normal days to 0.32 and 0.40 on E1 and E6, respectively. On contrary, a decrease in the ratio of nucleation mode particles to the total particles during haze episodes (0.09 and 0.05 during E1 and E6, respectively) was found, compared to that during normal days (0.13). The particle surface area concentration (PSC) and the particle volume concentration (PVC) showed significant increases during haze episodes, reaching 80–107% and 121–173% higher concentrations, respectively, than those on normal days. E1 started and ended with a NPF episode (Fig. 7a) during the relatively clean period, followed by low, sustained increase of PM_{2.5}. The NPF episodes observed in this study were driven by low atmospheric CS, high solar radiation, sunshine hours, and O₃. E1 were governed by meteorological conditions and characterized by two distinct aerosol formation processes of nucleation and growth. Decrease of SO₂ during increase phase of E6 were observed due to increasing RH favoring the transformation from precursor gas SO₂ to sulfate aerosols. The formation mechanism is aqueous SO₂ oxidation by NO₂ on fine aerosols. In addition, the results revealed that the temporal variations of N_{200–523} were similar to the trend of PM_{2.5} concentrations, indicating that N_{200–523} can be an indicator of haze episodes.

Acknowledgements

This study was supported by the National Natural Science Foundation of China (21107084) and the Special Foundation for State Major Research Program (51478386) from the Ministry of Science and Technology.

References

- Aalto, P., Hameri, K., Becker, E., Weber, R., Salm, J., Makela, J.M., Hoell, C., O'Dowd, C.D., Arnsson, H., Hansson, H.C., Vakeva, M., Koponen, I.K., Buzorius, G., Kulmala, M., 2001. Physical characterization of aerosol particles during nucleation events. *Tellus Ser. B: Chem. Phys. Meteor.* 53, 344–358.
- Asbach, C., Kaminski, H., Fissan, H., Monz, C., Dahmann, D., Mülhopt, S., Paur, H.R., Kiesling, H.J., Herrmann, F., Voetz, M., Kuhlbusch, T.A.J., 2009. Comparison of four mobility particle sizers with different time resolution for stationary exposure measurements. *J. Nanopart. Res.* 11, 1593–1609.
- Birmili, W., Wiedensohler, A., 2000. New particle formation in the continental boundary layer: meteorological and gas phase parameter. *J. Geophys. Res.* 27, 3325–3328.
- Cheng, Y.F., Zheng, G., Wei, C., Mu, Q., Zheng, B., Wang, Z., Gao, M., Zhang, Q., He, K., Carmichael, G., 2016. Reactive nitrogen chemistry in aerosol water as a source of sulfate during haze events in China. *Science Advances* 2 e1601530.
- Ding, Y., Liu, Y., 2014. Analysis of long-term variations of fog and haze in China in recent 50 years and their relations with atmospheric humidity. *Sci. China Earth Sci.* 57, 36–46.
- Guo, S., Hu, M., Zamora, M.L., Peng, J., Shang, D., Zheng, J., Du, Z., Wu, Z., Shao, M., Zeng, L., 2014. Elucidating severe urban haze formation in China. *Proc. Natl. Acad. Sci.* 111, 17373–17378.
- Hayakawa, I., 1964. The Effects of Humidity on the Coagulation Rate of ammonium chloride aerosols. *J. Air Pollut. Control Assoc.* 14 (9), 339–346. <https://doi.org/10.1080/00022470.1964.10468293>.
- Huang, R.J., Zhang, Y., Bozzetti, C., Ho, K.F., Cao, J.J., Han, Y., Daellenbach, K.R., Slowik, J.G., Platt, S.M., Canonaco, F., 2014. High secondary aerosol contribution to particulate pollution during haze events in China. *Nature* 514, 218–222.
- Jeong, C.H., Evans, G.J., 2009. Inter-comparison of a fast mobility particle sizer and a scanning mobility particle sizer incorporating an ultrafine water-based condensation particle counter. *Aerosol Sci. Technol.* 43, 364–373.
- Kulmala, M., Dal Maso, M., Makela, J.M., Pirjola, L., Vakeva, M., Aalto, P., Mikkulainen, P., Hameri, K., O'Dowd, C.D., 2001. On the formation, growth and composition of nucleation mode particles. *Tellus Ser. B: Chem. Phys. Meteor.* 53 (4), 479–490.
- Lee, B.P., Li, Y.J., Flagan, R.C., Lo, C., Chan, C.K., 2013. Sizing characterization of the fast-mobility particle sizer (FMPS) against SMPS and HR-ToF-AMS. *Aerosol Sci. Technol.* 47, 1030–1037.
- Li, H., Zhang, Q., Zhang, Q., Chen, C., Wang, L., Wei, Z., Zhou, S., Parworth, C., Zheng, B., Canonaco, F., Prévôt, A.S.H., Chen, P., Zhang, H., Wallington, T.J., He, K., 2017. Wintertime aerosol chemistry and haze evolution in an extremely polluted city of the North China Plain: significant contribution from coal and biomass combustion. *Atmos. Chem. Phys.* 17, 4751–4768.
- Lu, F., Xu, D., Cheng, Y., Dong, S., Guo, C., Jiang, X., Zheng, X., 2015. Systematic review

- and meta-analysis of the adverse health effects of ambient PM_{2.5} and PM₁₀ pollution in the Chinese population. *Environ. Res.* 136, 196–204.
- Ministry of Environmental Protection of the People's Republic of China (MEP), 2012a. Technical Regulation on Ambient Air Quality Index (AQI) (on Trial), HJ 633–2012. China Environmental Science Press, Beijing, China.
- Ministry of Environmental Protection of the People's Republic of China (MEP), 2012b. General Administration of Quality Supervision, Inspection and Quarantine of the People's Republic of China (AQSIQ), National Ambient Air Quality Standard (NAAQS), GB 3095–2012. China Environmental Science Press, Beijing, China.
- Peng, J.F., Hu, M., Wang, Z.B., Huang, X.F., Kumar, P., Wu, Z.J., 2014. Submicron aerosols at thirteen diversified sites in China: size distribution, new particle formation and corresponding contribution to cloud condensation nuclei production. *Atmos. Chem. Phys.* 14 (18), 10249–10265.
- Pirjola, L., Laaksonen, A., Aalto, P., Kulmala, M., 1998. Sulfate aerosol formation in the Arctic boundary layer. *J. Geophys. Res.* 103, 8309–8322.
- Shang, X., Zhang, K., Meng, F., Wang, S.H., Lee, M., Suh, I., Kim, D., Jeon, K., Park, H., Wang, X., Zhao, Y., 2018. Characteristics and source apportionment of fine haze aerosol in Beijing during the winter of 2013. *Atmos. Chem. Phys.* 18, 2573–2584.
- Shen, X.J., Sun, J.Y., Zhang, X.Y., Zhang, Y.M., Zhang, L., Che, H.C., Ma, Q.L., Yu, X.M., Yue, Y., Zhang, Y.W., 2015. Characterization of submicron aerosols and effect on visibility during a severe haze-fog episode in Yangtze River Delta, China. *Atmos. Environ.* 120, 307–316.
- Stanier, C.O., Khlystov, A.Y., Pandis, S.N., 2004. Nucleation events during the Pittsburgh air quality study: description and relation to key meteorological, gas phase, and aerosol parameters. *Aerosol Sci. Technol.* 38 (S1), 253–264.
- Tan, J.H., Duan, J.C., Zhen, N.J., He, K.B., Hao, J.M., 2016. Chemical characteristics and source of size-fractionated atmospheric particle in haze episode in Beijing. *Atmos. Res.* 167, 24–33.
- Wang, X.M., Chen, J.M., Cheng, T.T., Zhang, R.Y., Wang, X.M., 2014a. Particle number concentration, size distribution and chemical composition during haze and photochemical smog episodes in Shanghai. *J. Environ. Sci.* 26 (9), 1894–1902.
- Wang, Y.S., Li, Y., Wang, L.L., Liu, Z.R., Ji, D.S., Tang, G.Q., Zhang, J.K., Sun, Y., Hu, B., Xin, J.Y., 2014b. Mechanism for the formation of the January 2013 heavy haze pollution event over central and eastern China. *Sci. China Earth Sci.* 57, 14–25.
- Wang, H.L., An, J.L., Shen, L.J., Zhu, B., Pan, C., Lui, Z.R., Liu, X.H., Duan, Q., Liu, X., Wang, Y.S., 2014c. Mechanism for the formation and microphysical characteristics of submicron aerosol during heavy haze pollution episode in the Yangtze River Delta, China. *Sci. Total Environ.* 490 (15), 501–508.
- Wang, G., Zhang, R., Gomez, M.E., Yang, L., Zamora, M.L., Hu, M., Lin, Y., Peng, J., Guo, S., Meng, J., 2016. Persistent sulfate formation from London Fog to Chinese haze. *Proc. Natl. Acad. Sci.* 113, 13630–13635.
- Wang, Y.F., Chen, L., Chen, R., Tian, G.L., Li, D.X., Chen, C.Y., Ge, X.J., Ge, G.L., 2017a. Effect of relative humidity on the deposition and coagulation of aerosolized SiO₂ nanoparticles. *Atmos. Res.* 194 (15), 100–108.
- Wang, J., Zhang, J.S., Liu, Z.J., Wu, J.H., Zhang, Y.F., Han, S.Q., Zheng, X.J., Zhou, L.D., Feng, Y.C., Zhu, T., 2017b. Characterization of chemical compositions in size-segregated atmospheric particles during severe haze episodes in three mega-cities of China. *Atmos. Res.* 187, 138–146.
- Wang, G.H., Zhang, F., Peng, J.F., Duan, L., Ji, Y.M., Marrero-Ortiz, W., Wang, J.Y., Li, J., Wu, C., Cao, C., Wang, Y., Zheng, J., Secret, J., Li, Y.X., Wang, Y.Y., Li, H., Li, N., Zhang, R.Y., 2018. Particle acidity and sulfate production during severe haze events in China cannot be reliably inferred by assuming a mixture of inorganic salts. *Atmos. Chem. Phys.* 18, 10123–10132.
- WHO Regional Office for Europe, 2005. Air Quality Guideline: Global Updates. vol. 2006.
- Yang, Y., Liu, X., Qu, Y., Wang, J., An, J., Xiang, Y., Xiang, F., 2013. Formation mechanism of continuous extreme haze episodes in the megacity Beijing, China. *Atmos. Res.* 155, 192–203.
- Zhang, R., Khalizov, A., Wang, L., Hu, M., Xu, W., 2011. Nucleation and growth of nanoparticles in the atmosphere. *Chem. Rev.* 112, 1957–2011.
- Zhang, X.Y., Wang, Y.Q., Niu, T., Zhang, X.C., Gong, S.L., Zhang, Y.M., Sun, J.Y., 2012. Atmospheric aerosol compositions in China: spatial/temporal variability, chemical signature, regional haze distribution and comparisons with global aerosols. *Atmos. Chem. Phys.* 12, 779–799.
- Zhang, Q., Quan, J., Tie, X., Li, X., Liu, Q., Gao, Y., Zhao, D., 2015a. Effects of meteorology and secondary particle formation on visibility during heavy haze events in Beijing, China. *Sci. Total Environ.* 502, 578–584.
- Zhang, R., Wang, G., Guo, S., Zamora, M.L., Ying, Q., Lin, Y., Wang, W., Hu, M., Wang, Y., 2015b. Formation of urban fine particulate matter. *Chem. Rev.* 115, 3803–3855.
- Zhang, Y., Huang, W., Cai, T.Q., Fang, D.Q., Zhang, Y.X., 2016. Concentrations and chemical compositions of fine particles (PM_{2.5}) during haze and non-haze days in Beijing. *Atmos. Res.* 174–175, 62–69.
- Zhao, X.J., Zhao, P.S., Xu, J., Meng, W., Pu, W., Dong, F., He, D., Shi, Q.F., 2013. Analysis of a winter regional haze event and its formation mechanism in the North China Plain. *Atmos. Chem. Phys.* 13, 5685–5696.
- Zimmerman, N., Jeong, C.H., Wang, J.M., Ramos, M., Wallace, J.S., Evans Greg, J., 2015. A source-35 independent empirical correction procedure for the fast mobility and engine exhaust particle sizers. *Atmos. Environ.* 100, 178–184.